Partial glass isosymmetry transition in multiferroic hexagonal $ErMnO_3$

A. Barbour,[1,*] A. Alatas,[2] Y. Liu,[1] C. Zhu,[1] B. M. Leu,[2] X. Zhang,[2] A. Sandy,[2] M. S. Pierce,[3] X. Wang,[4] S.-W. Cheong,[4] and H. You[1,†]

[1]*Materials Science Division, Argonne National Laboratory, Argonne, Illinois 60439, USA*
[2]*Advanced Photon Source, Argonne National Laboratory, Argonne, Illinois 60439, USA*
[3]*Department of Physics, Rochester Institute of Technology, Rochester, New York 14623, USA*
[4]*Rutgers Center for Emergent Materials and Department of Physics and Astronomy, Rutgers University, Piscataway, New Jersey 08854, USA*

(Received 14 April 2015; revised manuscript received 27 January 2016; published 18 February 2016)

Ferroelectric transitions of a hexagonal multiferroic, $ErMnO_3$, are studied by x-ray scattering techniques. An isosymmetry transition, similar to that previously observed for $YMnO_3$, approximately 300 K below the well-known ferroic transition temperature, is investigated. The partially glassy behavior of the isosymmetry transition is identified by the appearance of quasielastic scattering lines in high-energy-resolution scans. The glassy behavior is further supported by the increased interlayer decorrelation of $(\sqrt{3} \times \sqrt{3})R30^\circ$ ordering below the isosymmetry transition. The transition behavior is considered for possible hidden sluggish modes and two-step phase transitions theoretically predicted for the stacked triangular antiferromagnets. The in-plane azimuthal (orientational) ordering behaviors were also compared to the theoretical predictions. Coherent x-ray speckle measurements show unambiguously that the domain sizes decrease anomalously near both the isosymmetry and ferroic transitions. However, domain boundary fluctuations increase monotonically with an Arrhenius form with an activation energy of 0.54(5) eV through both transitions.

DOI: 10.1103/PhysRevB.93.054113

I. INTRODUCTION

Multiferroics are of scientific and technological interest for coupling of magnetism and ferroelectricity [1]. Among them, layered hexagonal manganites exhibit unit-cell tripling transitions and the trimerization leads to intricate vortices and domains [2] The magnetizations are strongly coupled at domain walls due to the improper coupling of trimerization [3] to the ferroelectric order parameters [4], and some exhibit room-temperature multiferroic behavior [5]. While it is well recognized [2,4] that the trimerization is key to the multiferroic behavior, the process of the trimerization, the ferroic (para-ferro) transition is not well understood. Although the hex-manganites were discovered long ago [6,7], it is still under extensive investigation how the high-temperature para phase transforms to the low-temperature trimerized phase and whether or not there should be an intermediate transition [8–14]. We examined single crystals of $ErMnO_3$ (and $YMnO_3$) [15] with x-ray techniques to elucidate the structural and dynamical aspects of the trimerization transitions.

At high temperatures, $ErMnO_3$ forms a simple hexagonal para phase with $P6_3/mcm$ symmetry. At T_c (1195ºC), one of three Er atoms buckles out of the plane, forming an antiferroelectric $(\sqrt{3} \times \sqrt{3})R30^\circ$ superlattice with concomitant tilting of MnO_5 bipyramids (trimerization), which lowers the symmetry to $P6_3cm$ [16]. In addition, hundreds of degrees below T_c, an intermediate transition has been suggested in the thermal expansion measurements on $YMnO_3$ by Nénert *et al.* [10]. However, the neutron powder diffraction study by Gibbs *et al.* [14] did not find a symmetry change, which is expected in a real phase transition. Instead, the study found that some structure parameters, such as the total polarization, decrease suddenly and hence this is termed an isosymmetry transition. Our *in situ* equilibrium measurements were started with the as-grown $ErMnO_3$ single crystals and repeated by cycling above the ferroic transition temperature where domain patterns are expected to evolve [2,17,18]. We find also hundreds of degree below T_c that the intensities of quasielastic lines, in nonresonant high-energy-resolution inelastic x-ray scattering (HERIX), exhibit a transition indicating a rapid change in the dynamic nature, much like a glass transition. Other characteristics further supporting the glassy behavior of the transitions are also studied using conventional x-ray techniques. In addition, the domain statics and dynamics are studied with coherent x-ray speckle scattering measurements, where the K_3-mode activation energy at the domain boundary is obtained. Our studies are compared to theoretical studies with the Landau expansion [19] of the proposed hidden order parameter [20] for a possible origin of the glass transition behavior and a recent Monte Carlo (MC) simulation [21] where orientational order parameters are investigated.

II. EXPERIMENT

$ErMnO_3$ (and $YMnO_3$) crystal specimens were grown by a flux method: 10 mol% of the corresponding polycrystalline powder with 90 mol% Bi_2O_3 powder as flux were heated to 1250°C, and then slowly cooled to 800°C in a platinum crucible. The samples consisted of plates of 1–3 mm and ∼0.1mm in thickness. The surfaces of the samples were (001) planes without exception. The fresh samples are shiny, reflecting ambient light with few defects. In fact, the fresh surfaces exhibit well-defined atomic step structures [15]. However, the samples can lose the luster over the course of

*Current address: Brookhaven National Laboratory, National Synchrotron Light Source II, Upton, NY 11973, USA.
†Author to whom correspondence should be addressed: hyou@anl.gov

several days in air at high temperature. This was much more evident in $YMnO_3$ samples [15]. For this reason, $YMnO_3$ was not as much studied here as $ErMnO_3$.

Samples were affixed with a thin layer of high-temperature paste on a 1 cm cylindrical platinum crystal that is inductively heated to a desired temperature. The sample temperature was measured with a *K*-type thermocouple spot welded to the platinum crystal and additionally calibrated by the platinum thermal expansion. Finally the temperature of the sample was calibrated against the platinum temperature using a pyrometer. We estimate the accuracy of the absolute temperature is limited by the pyrometer readings of the sample and platinum to $\pm 25^\circ$ and the relative accuracy is limited by the thermocouple to $\pm 5^\circ$.

X-ray integrated-intensity measurements and H and L scans were performed with in-house rotating anode x rays. Lattice constant measurements, coherent x-ray scattering, and HERIX measurements were performed at 11ID-D, 8ID-E, and 3ID-C beamlines, respectively, at the Advanced Photon Source (APS), Argonne National Laboratory. The lattice constants were measured with a wavelength of 1.07812 Å. A Pilatus 100K, which has 200(horizontal)×1000(vertical) pixels with a pixel size of 0.175 mm, was used as a detector. The region of interest was set to two pixels vertically to maintain ∼0.4 mrad resolution in the vertical 2θ scan direction, while the detected intensities along the other directions are integrated. The *a*-axis lattice constant was measured with the (1 1 0.15) off-specular reflection in a glancing-incidence geometry. Because the thin sample was affixed with paste to the platinum crystal surface for heating, access to an in-plane peak was possible only in glancing-incidence reflection geometry. HERIX experiments were performed using an energy-variable six-bounce monochromator at the x-ray energy of 21.657 keV [22]. Fixed backscattering analyzers were used, achieving ∼2 meV energy resolution [23]. Four analyzers, spaced at fixed $\Delta 2\theta$ angular distances, were mounted on the horizontally scanning 2θ arm for simultaneous data acquisition. Coherent x-ray experiments were performed with a single-bounce Si (111) monochromator, setting the photon energy to 7.36 keV. The beam was vertically focused to 3 μm by a kinoform [24] lens with the acceptance of ∼100 μm set by vertical slits and horizontally unfocused to the size of 10 μm set by horizontal slits. This beam profile delivers a sufficient transverse coherence for reflection coherent x-ray experiments where the pathlength differences from the surface layers are much less than the longitudinal coherence length. The detector was an x-ray-sensitive charge-coupled device with a pixel size of 25 μm and mounted on the 2θ arm at a distance of 1 m from the sample. The correlation time in our reflection experiment with a static sample was over 10^5 s [25,26].

III. RESULTS AND DISCUSSION

The lattice expansion measured in synchrotron high-momentum-resolution measurements shows an anisotropic behavior. The measured *a* and *c* lattice parameters are shown in Fig. 1 with the known room-temperature lattice constants [3]. The *a* lattice constant (left abscissa) expands without any hint of the intermediate transition. In fact, there is no hint of a transition even at T_c, and a straight line can be

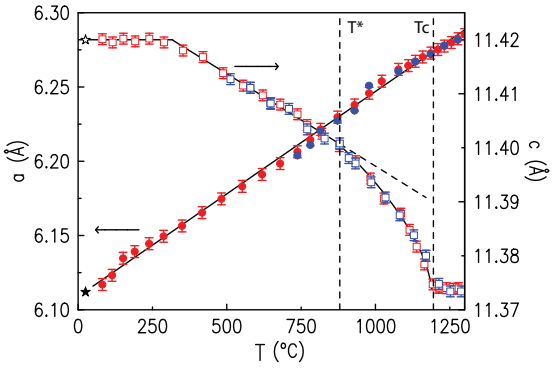

FIG. 1. Lattice constants of $ErMnO_3$, *a* (filled circles) and *c* (open squares), measured in heating (red symbols) and in cooling (blue symbols). The filled and open stars at 25ºC are from [Ref. [3]]. The thermal expansion rate of *a* is $1.38(2) \times 10^{-4}$ and that of *c* varies from 0 to -6×10^{-5}.

fitted over the entire temperature range that we measured. Yet there are interesting features in the *c* lattice constant (right abscissa): little or slow expansion up to ∼350ºC, linear *contraction*, not expansion, to 880ºC, acceleration of the contraction between 880ºC and T_c, and no further contraction above T_c. This indicates that only *c*-axis negative expansion is sensitive to phase transitions while the *a* axis is unaffected by the transitions and follows a linear thermal expansion. This anisotropic expansion behavior and the slope discontinuity [27] at 880ºC provide initial clues for understanding the transition behaviors.

The tripling order parameter, measured by the intensity of the (1 0 4) reflection, shows an anomaly at 880ºC, otherwise exhibiting a power-law behavior. In x-ray scattering measurements, because the scattering factor of Er is much larger than those of Mn and O, the buckled Er atoms contribute primarily to the unit-cell tripling reflections such as (1 0 *L*). The intensity is proportional to $|\delta L|$ [2], where δ is the out-of-plane distance between Er atoms, and represents the square of the corresponding order parameter, which in turn closely resembles the antiferroelectric order parameter [12]. On close examination of the (1 0 *L*) intensities, we found that the intensity of the (1 0 *L*) reflection does not change monotonically even though the behavior close to T_c follows a power law. This is evident in the (1 0 4) reflection shown in Fig. 2(a). We find that the (1 0 4) intensity near T_c between 900 and 1195°C is fitted very well with the function $\propto(1195-T)^{2\beta}$ with $\beta = 0.25(1)$ (black solid line). However, the (1 0 4) intensity deviates significantly from the solid line below 900°C where we found the *c*-lattice-constant (Fig. 1) slope discontinuity. Therefore, we drew another solid line with a similar function (blue line), $\propto (880 - T)^{0.5}$. Henceforth, we tentatively denote this intermediate isosymmetry transition [14] at 880ºC as T^* [21].

Below the T^* transition, the quasielastic line intensity *increases* as temperature *decreases*. Selected HERIX scans at (1.05 0 4) and (0.75 0 2.95) are shown in Figs. 3(a) and 3(b), respectively. (1.05 0 4) is chosen to be near but not precisely at (1 0 4) and (0.75 0 2.95) is the position of one of the three accompanying detectors [22] chosen for the odd *L* value (2.95≈3). In both cases, there are unusually large

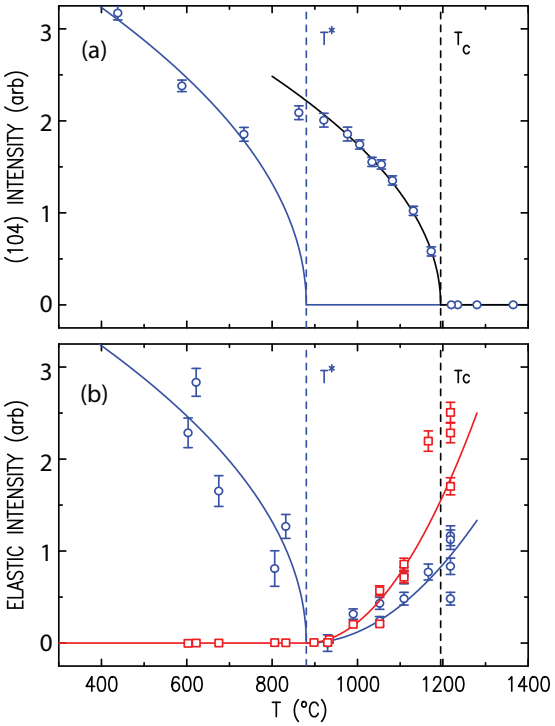

FIG. 2. (a) Integrated intensity of (1 0 4) vs T. (b) Quasielastic Intensity vs T at (1.05 0 4) (circles) and (0.75 0 2.95) (squares).

central quasielastic peaks, in both (a) and (b), albeit truncated to show the transition better. The integrated intensities of the quasielastic peaks are summarized in Fig. 2(b) with a solid line of the function $\propto (880 - T)^{0.5}$. The quasielastic peak appears at T^* and its intensity increases as T decreases. The quasielastic peak intensity is expected to be zero or weak away from Γ (Bragg) points for ideal lattices. The strong quasielastic peak indicates that there are static, frozen, overdamped, or sluggish modes because the quasielastic x-ray measurements are essentially long-exposure averages of the corresponding Fourier component over picoseconds or longer. We find at room temperature that the quasielastic intensity of $(1\pm\eta\ 0\ 4)$ drops rapidly as η ($\eta \ll 1$) increases, indicating that the frozen or sluggish modes are due to imperfect $(\sqrt{3}\times\sqrt{3})R30^\circ$ ordering. The amplitudes of frozen or sluggish modes are large at low temperature and the modes gradually unfreeze at T^* as T increases, much like the behavior of a glass. This behavior is also similar to the behavior of $Pb(Mn_{1/3},Nb_{2/3})O_3$ [28], a prototypical relaxor. The frozen imperfections most likely suppress the Γ_2^- mode, which is a primary ferroelectric mode along the c axis [14]. When the imperfections disappear, the (1 0 4) Bragg intensity jumps back up near T^* in Fig. 2(a) and the $(\sqrt{3}\times\sqrt{3})R30^\circ$ ordering is partially restored. In Fig. 3(b) of the energy scans at (0.75 0 2.95), the quasielastic peaks are weak because the quasielastic intensity at the odd L value is independent of c-axis disordering. The glassy behavior disappears above T^*. Both quasielastic intensities increase with $(T - T^*)^2$. This happens when the interlayer stacking order is high near T^* but gradually decreases as T increases. The increase of the quasielastic peak intensity, $\propto (T - T^*)^2$, indicates that the interlayer misalignment vector ε increases with T since $I_{\text{misfit}} \propto |\varepsilon Q|^2$ for small misalignments [28]. The continued increase even above T_c indicates that short-range Er buckling still exists, as for Y atoms [14].

The increased stacking correlation near T^* is additionally confirmed in conventional diffraction experiments. In Fig. 4(a), we show the measured full width at half maximum (FWHM) of L scans through the (1 0 4) reflection vs T with squares. We find that the FWHM decreases almost to that of the instrumental resolution, ~0.01 reciprocal lattice units (r.l.u.) as $T \to T^*$. From the width, we calculated the correlation length (circles) using the relation $\xi = c\,2\sqrt{2\ln 2}/\sqrt{(\sigma^2 - \sigma_0^2)}$ where ξ, σ, and σ_0 are the correlation length, the FWHM, and the instrumental resolution, respectively. The fits to the L scans were made with a pseudo-Voigt function. However, the Lorentzian component was small and did not change much over the entire temperature range. The fit shows that the interlayer stacking correlation length diverges at T^*. The widths of in-plane radial and azimuthal scans are shown in Fig. 4(b). The widths of the azimuthal scans behave similarly to those of the L scans albeit being somewhat more complex. Note that the widths of the radial scans do not change significantly over the same temperature range. (The weak T dependence seen here is largely due to the resolution envelope overlapping with the azimuthal scans.) Again, we show that the interlayer correlations are low (large widths) at low temperature and increase as T increases to T^*, which is opposite to the property of ordinary crystalline materials and the prediction of a recent MC study [21]. This is significant because the MC prediction agrees well with our results above T^* [see Fig. 4(b)] when the behavior returns to that of ordinary crystalline materials. Namely, the interlayer stacking azimuthal correlation drops (the azimuthal width increases) significantly as expected approaching T_c. Below T^*, however, we believe it does so because the azimuthal correlation has glassy behavior.

Consideration of the anisotropic lattice expansion, quasielastic intensity, and scan widths discussed above suggests that the stacking correlation of the superstructure changes at T^* with little or no in-plane superstructure disorder. One way to elucidate the nature of the two-step transition behavior is to compare with previous phase-transition studies. Based on the behavior of the transition near T_c, we expect that the transition is second order or weakly first order. In mean-field terminology, this value of β indicates a critical transition through the tricritical point. This is unlikely and we may consider the transition behavior beyond the mean-field approximation by mapping the Er displacement to Ising magnets on a stacked triangular lattice. Ising magnets on a stacked triangular lattice represent a frustrated system and have been studied theoretically [29,30] and experimentally [31]. In particular, a Monte Carlo $S = \infty$ simulation study [32] is interesting as the magnetization $|M|$ exhibits a two-step transition that is qualitatively similar to T^* and T_c seen in the (1 0 4) intensity [Fig. 2(a)]. The two steps are a transition from the ferrimagnetic (FR) structure to a partially disordered (PD) structure at $k_B T^*/J = 0.8$ and another from PD to paramagnetization at $k_B T_c/J = 1.2$. In addition, our exponent $\beta = 0.25$ is in remarkable agreement with the theoretical study [30] that is confirmed in the neutron diffraction experiments [31]. Another critical exponent $\nu = 0.53$ of the model [30] can also be considered as indicated by the solid red line in Fig. 4, $\xi = \alpha(1 - T/880)^{-\nu}$, with the fit value of $\alpha = 1.7(1) \times 10^2$ Å.

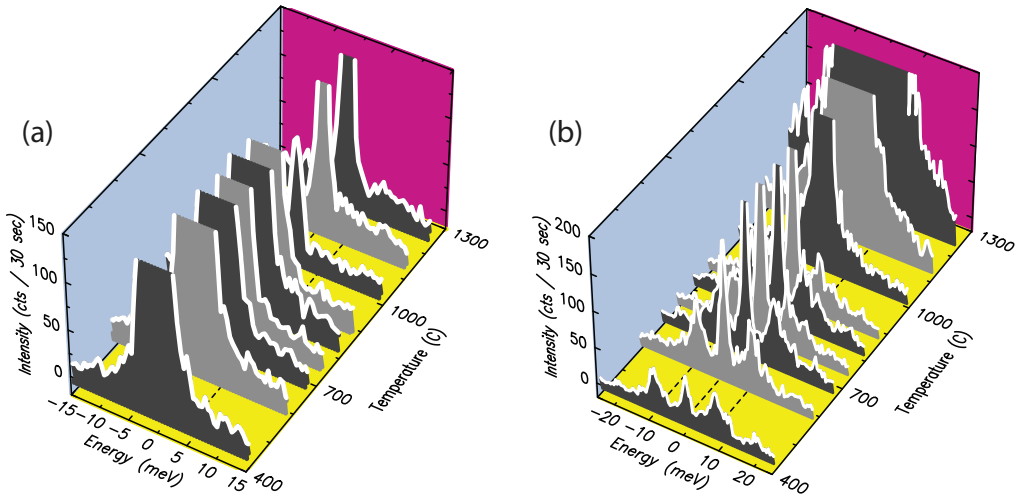

FIG. 3. HERIX scans at (1.05 0 4) (a) and (0.75 0 2.95) (b). The dashed lines are at 0 and ±8 meV. The intensities are truncated at 150 and 200 counts per 30 s for clarity.

Therefore, we believe that the model of stacked triangular antiferromagnets is a good approach. It will be of theoretical interest to further explore dynamic and critical behaviors of the hexagonal antiferroelectrics by considering some differences.

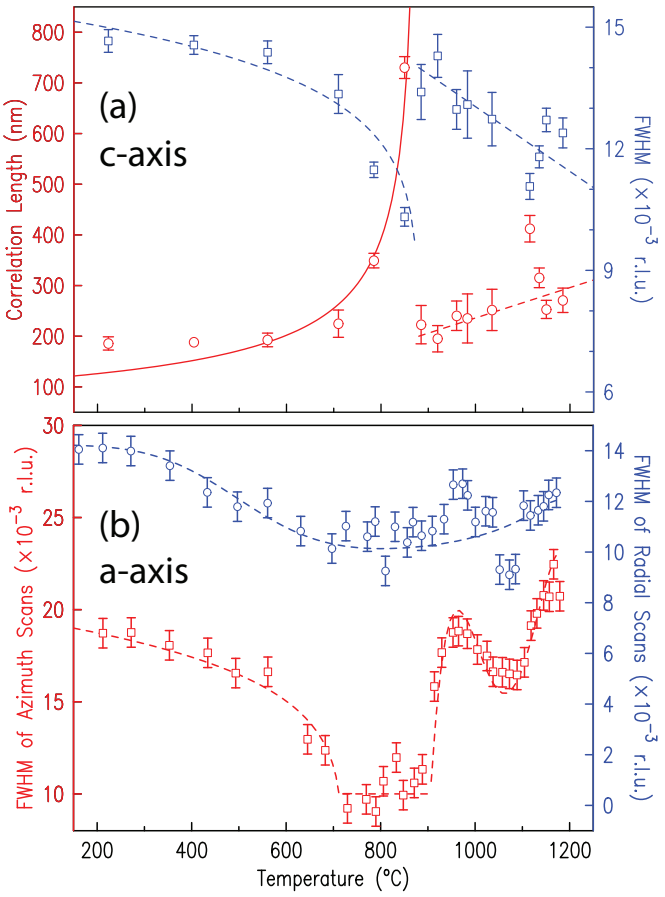

FIG. 4. Scan widths of (1 0 4) along the L (a), H (b, circles), and $H - 2\bar{H}$ (b, squares) directions plotted vs T. The solid red line in (a) is a power law with the exponent $\nu = 0.53$ [29]. The dashed lines are guides to the eye.

$ErMnO_3$ has an A-B stacked hexagonal lattice, not an A-A triangular lattice. More importantly, the antiferroectric trimerization must be accompanied by MnO_5 bipyramids linking the interlayer positions of the Er trimerization, which leads to internal disordering. In fact, the possible three Er states proposed by Cano [20] can reinforce the relationship to the layered triangular antiferromagnets. In this regard, the glassy aspect of the observed behavior can be considered from the perspective of short-range hidden or complex order parameter(s) [20]. While the overall averaged structure has well-defined symmetry, unitcells, and atomic positions, we have shown that certain modes undergo a glasslike transition behavior, evident in the dynamics of the system and probably due to the complex nature of the trimerization. On the other hand, it could simply be like the glass transition [30], which is often characterized by dynamic behavior without identifiable specific mode(s), or with many modes entangled to form a glassy state similar to spin-glass-type disordering [33,34]. In a way, our observations suggest that an apparently well-defined structure in the classical sense may not be as well defined as we thought. The glassy state also explains the sudden decrease in the total polarization [14].

While the above incoherent x-ray techniques are insensitive to domain boundaries, coherent x rays are sensitive to the domain boundaries and their fluctuations. It is well established that $ErMnO_3$ crystals form complex topological domains and the domain sizes and shapes are sensitive to the cooling rate [17] that is accessible within the time scales of x-ray photon correlation spectroscopy (XPCS) [35]. We used the surface-sensitive speckle patterns on a crystal truncation rod (CTR) [25,36,37]. The CTR x-ray speckles arise from interferences between structure factors of up (+) and down (−) terminations [38–40]. A simple derivation [15] yields the CTR structure factor for a fixed l from a mix of + and − domains as

$$S_{\mathrm{CTR}}(l,p,q) = \frac{f^{+}e^{i\Delta\varphi}}{1-e^{-i2\pi l}} \iint_{S^{+}} e^{-i(px+qy)}dxdy,$$

where f^{+} and $\Delta\varphi$ are the amplitude of the + domain and the phase difference between + and − domains, p and q are the momentum transfers of a given pixel, and S^{+} represents

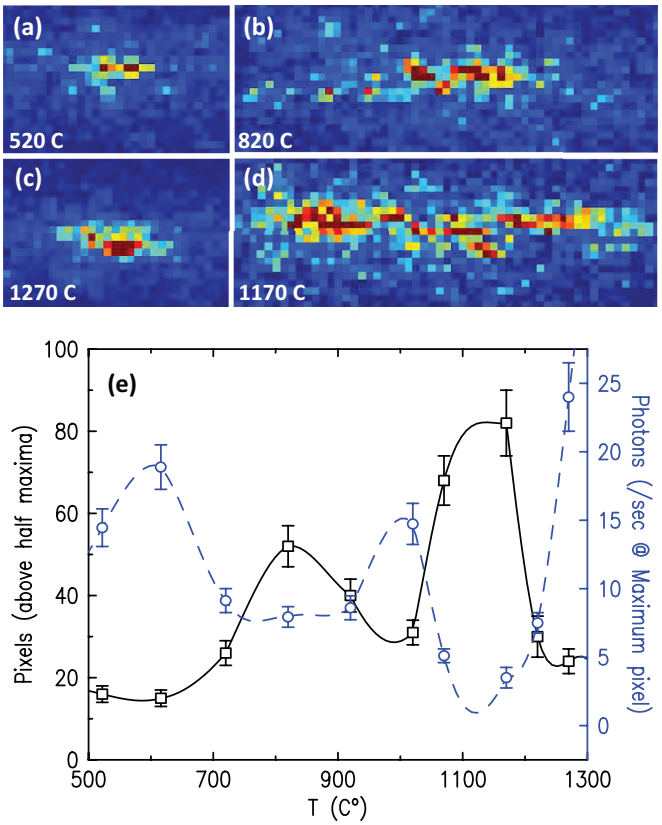

FIG. 5. (a)–(d) Speckles measured at the noted temperatures. (e) Squares are numbers of the pixels above the half maxima and the circles are peak intensities per pixel averaged from four pixels of highest intensities. The lines are guides to the eye.

the fragmented area [2] of the + domains. The calculated phase difference [15] is almost π near (0 0 4) and S_{CTR} is proportional to $2f^{+}/2\pi\Delta l$ times the integral. Note that the speckle pattern changes when domain boundaries meander or reshape. Therefore, the time evolution of speckles is a result of domain boundary meandering while the speckle pattern is a result of domain sizes and distributions. A point of the CTR, (0 0 4.125), was chosen for strong enough intensity for XPCS analysis and sufficient sensitivity to near-surface domain structures ($\Delta l = 1/8$, eight unit cells, or ~10 nm deep) [15].

The two-step transitions are also evident in domain dynamics measured with coherent x-ray speckles. Examples of speckle patterns are shown in Figs. 5(a)–5(d). The green pixels are at half maxima and the red and yellow pixels are above. In Fig. 5(e), the peak intensities (circles) and full area at half maxima (FAHM) (squares) are plotted. While the integrated intensity (peak intensity times the FAHM) shows no significant change over the temperature range, the FAHM increases greatly near both T^* and T_c and drops down between them. This can also be seen from the images in Fig. 5(b) at 820°C and (d) at 1170°C where speckles spread, indicating that domain sizes are smaller below both transitions. The domains are much smaller near the ferroic transition as expected. Note, however, that spread speckles, namely, small domains, from the near-surface region at 820°C do not necessarily mean smaller domains on average since the interlayer correlation is high near T^*.

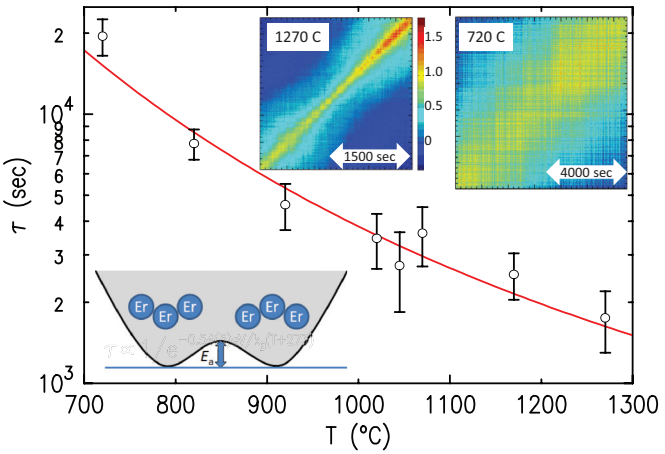

FIG. 6. Correlation time of domain boundary dynamics plotted against temperature. The solid line is the fit with the activation energy of 0.54(5) eV. The upper insets are two-time correlations for 1270°C and 720°C and the lower inset shows schematically configurations of Er positions and the activation energy.

The temporal behavior of the domain boundary motions can be characterized by a single thermodynamic parameter τ, the correlation time, using XPCS autocorrelation analysis [35]. We plot τ vs temperature in Fig. 6. The value of τ changes by more than an order of magnitude from ~20000 s at 720°C to <2000 s at 1270°C. The two-time correlation maps are also shown as insets, where we can clearly compare two temperatures. The diagonal high intensity indicates that the pattern self-correlates while the off-diagonal spread indicates how rapidly the pattern decorrelates in time. A lay-term interpretation of τ, therefore, is the time elapsed for a domain pattern to lose most of the resemblance to the initial pattern due to the domain boundary meandering. For a domain boundary to meander, of course, the Er atom must overcome the activation potential (see the lower inset) between the up and down domains with appropriate adjustment of the MnO_3 polyhedron. This is essentially equivalent to the K_3 phonon activation energy per unit cell. In a simple thermodynamic activation processes, we have shown that τ follows a simple Arrhenius form [25,41]. This is also true here as shown in Fig. 6 with the activation energy of 0.54(5) eV. This is remarkable because the domain sizes change nonmonotonically as in Fig. 5(e). This apparently counterintuitive observation has in fact a quite simple interpretation. The domain boundary energy decreases at the phase transitions while the activation energy of moving the domain boundaries remains constant over the entire temperature ranges of the two transitions. It is also remarkable to see that the activation energy agrees well with the result of the *ab initio* calculation where the energy barrier of the K_3 mode between the amplitudes of 0 Å and 0.85 Å (energy minimum) is ~0.5 eV [19] when the energies are renormalized by the ratio of the T_c's for $ErMnO_3$ and $YMnO_3$.

IV. SUMMARY

In summary, we report an observation of partially glassy behavior of the isosymmetry dynamic phase transition of $ErMnO_3$. The dynamic nature of the transition is

unambiguously defined in high-energy-resolution quasielastic x-ray measurements supported by interlayer correlation-length measurements. The transition appears consistent with critical behavior of stacked triangular antiferromagnets above the transition (T^*). However, the low-temperature behavior below the transition is much like that of glasses even though the average structure is well described by the $P6_3cm$ symmetry. We propose that the system behaves like stacked triangular spin glasses where the random interactions are provided by MnO_5 interlinking bipyramids, probably controlled by hidden order parameters [20]. We believe that similar partial glass transitions likely exist in other multiferroics, and probably in other complex materials such as relaxor ferroelectrics [42] where the relevant phonon modes [28,43] are still under investigation. We also find that both isosymmetry and ferroic transitions have a strong influence on the domain structures in our coherent x-ray scattering studies. Our x-ray photon correlation spectroscopy analysis of the speckle patterns finds the K_3-mode activation energy of $ErMnO_3$ to be 0.54(5) eV.

ACKNOWLEDGMENTS

The work of A.B., C.Z., and H.Y. at Materials Science Division at Argonne National Laboratory was supported by the U.S. Department of Energy (DOE), Office of Basic Energy Sciences (BES), Materials Sciences and Engineering Division (MSED), and the work of A.A., B.L., A.S., and X.Z. at the Advanced Photon Source (APS) and use of the APS by DOE BES Scientific User Facilities Division (SUFD), under Contract No. DE-AC02-06CH11357. The work at Rutgers was funded by the DOE under Grant No. DE-FG02-07ER46382.

[1] S.-W. Cheong and M. Mostovoy, Nat. Mater. **6**, 13 (2007).
[2] T. Choi, Y. Horibe, H. T. Yi, Y. J. Choi, W. Wu, and S.-W. Cheong, Nat. Mater. **9**, 253 (2010).
[3] B. B. van Aken, T. T. M. Palstra, A. Fillippetti, and N. A. Spaldin, Nat. Mater. **3**, 164 (2004).
[4] H. Das, A. L. Wysocki, Y. Geng, W. Wu, and C. J. Fennie, Nat. Commun. **5**, 2998 (2014).
[5] W. Wang, J. Zhao, W. Wang, Z. Gai, N. Balke, M. Chi, H. N. Lee, W. Tian, L. Zhu, X. Cheng, D. J. Keavney, J. Yi, T. Z. Ward, P. C. Snijders, H. M. Christen, W. Wu, J. Shen, and X. Xu, Phys. Rev. Lett. **110**, 237601 (2013).
[6] H. L. Yakel, W. C. Koehler, E. F. Bertaut, and E. F. Forrat, Acta. Crystallogr. **16**, 957 (1963).
[7] Ph. Coeuré, F. Guinet, J. C. Peuzin, G. Buisaon, and E. F. Bertant, in *Proceedings of the International Meeting on Ferroelectricity*, held at Prague (1966) in two volumes, edited by V. Dvorak, A. Fouskova, and P. Glogar (Inst. of Phys. of the Czeckoslovak Acad. of Sci. Prague, 1966), Vol. 1, p. 332.
[8] Th. Lonkai, D. G. Tomuta, U. Amann, J. Ihringer, R. W. A. Hendrikx, D. M. Többens, and J. A. Mydosh, Phys. Rev. B **69**, 134108 (2004).
[9] I.-K. Jeong, N. Hur, and Th. Proffen, J. Appl. Crystallogr. **40**, 730 (2007).
[10] G. Nénert, M. Pollet, S. Marinel, G. R. Blake, A. Meetsma, and T. T. M Palstra, J. Phys.: Condens. Matter **19**, 466212 (2007).
[11] J. Kim, Y. M. Koo, K.-S. Sohn, and N. Shin, Appl. Phys. Lett. **97**, 092902 (2010).
[12] C. J. Fennie and K. M. Rabe, Phys. Rev. B **72**, 100103(R) (2005).
[13] J. Varignon, S. Petit, and M.-B. Lepetit, arXiv:1203.1752.
[14] A. S. Gibbs, K. S. Knight, and P. Lightfoot, Phys. Rev. B **83**, 094111 (2011).
[15] See Supplemental Material at http://link.aps.org/supplemental/10.1103/PhysRevB.93.054113 for preliminary characterizations of the samples, mathematical derivations for the equation, energy-resolution measurements, and the related measurements of $YMnO_3$.
[16] B. B. Van Aken, A. Meetsma, and T. T. M. Palstra, Acta Crystallogr. **E57**, i38 (2001).
[17] S. C. Chae, N. Lee, Y. Horibe, M. Tanimura, S. Mori, B. Gao, S. Carr, and S.-W. Cheong, Phys. Rev. Lett. **108**, 167603 (2012).
[18] S. C. Chae, Y. Horibe, D. Y. Jeong, S. Rodan, N. Lee, and S.-W. Cheong, Proc. Natl. Acad. Sci. USA **107**, 21366 (2010).
[19] S. Artyukhin, K. T. Delaney, N. A. Spaldin, and M. Mostovoy, Nat. Mater. **13**, 42 (2013).
[20] A. Cano, Phys. Rev. B **89**, 214107 (2014).
[21] M. Lilienblum, T. Lottermoser, S. Manz, S. M. Selbach, A. Cano, and M. Fiebig, Nat. Phys. **11**, 1070 (2015).
[22] T. S. Toellner, A. Alatas, and A. H. Said, J. Synchrotron Radiat. **18**, 605 (2011).
[23] A. Alatas, B. M. Leu, H. Yavas, T. S. Toellner, and E. E. Alp, Nucl. Instrum. Methods Phys. Res., Sect. A **649**, 166 (2011).
[24] A. F. Isakovic, A. Stein, J. B. Warren, S. Narayanan, M. Sprung, A. R. Sandy, and K. Evans-Lutterodt, J. Synchrotron Radiat. **16**, 8 (2009).
[25] M. S. Pierce, K.-C. Chang, D. C. Hennessy, V. Komanicky, M. Sprung, A. Sandy, and H. You, Phys. Rev. Lett. **103**, 165501 (2009).
[26] M. S. Pierce, V. Komanicky, A. Barbour, D. C. Hennessy, C. Zhu, A. Sandy, and H. You, Phys. Rev. B **86**, 085410 (2012).
[27] The slope discontinuity is related to the heat capacity of a transition via Grüneisen parameters. See H. You *et al.*, Phys. Rev. B **38**, 9213 (1988); **43**, 3660 (1991).
[28] H. You and Q. M. Zhang, Phys. Rev. Lett. **79**, 3950 (1997).
[29] D. Blankschtein, M. Ma, A. N. Berker, G. S. Grest, and C. M. Soukoulis, Phys. Rev. B **29**, 5250 (1984).
[30] H. Kawamura, J. Phys. Soc. Jpn. **54**, 3220 (1985).
[31] Y. Ajiro, T. Nakashima, Y. Unno, H. Kadowaki, M. Mekata, and N. Achiwa, J. Phys. Soc. Jpn. **57**, 2648 (1988).
[32] O. Nagai, M. Kang, T. Horiguchi, and H. T. Diep, Phys. Lett. A **186**, 359 (1994).
[33] K. Binder and A. P. Young, Rev. Mod. Phys. **58**, 801 (1986).
[34] L. Berthier and G. Biroli, Rev. Mod. Phys. **83**, 587 (2011).
[35] D. Lumma, L. B. Lurio, S. G. J. Mochrie, and M. Sutton, Rev. Sci. Instrum. **71**, 3274 (2000).
[36] I. K. Robinson, Phys. Rev. B **33**, 3830 (1986).

[37] I. A. Vartanyants, J. A. Pitney, J. L. Libbert, and I. K. Robinson, Phys. Rev. B **55**, 13193 (1997).
[38] Speckles are insensitive to the topological boundaries between α, β, and γ domains.
[39] I. K. Robinson, W. K. Waskiewicz, R. T. Tung, and J. Bohr, Phys. Rev. Lett. **57**, 2714 (1986).
[40] H. You, U. Welp, G. W. Crabtree, Y. Fang, S. K. Sinha, J. D. Axe, X. Jiang, and S. C. Moss, Phys. Rev. B **45**, 5107 (1992).
[41] M. S. Pierce, D. C. Hennessy, K.-C. Chang, V. Komanicky, J. Strzalka, A. Sandy, A. Barbour, and H. You, Appl. Phys. Lett. **99**, 121910 (2011).
[42] V. Westphal, W. Kleemann, and M. D. Glinchuk, Phys. Rev. Lett. **68**, 847 (1992).
[43] I. P. Swainson, C. Stock, P. M. Gehring, Guangyong Xu, K. Hirota, Y. Qiu, H. Luo, X. Zhao, J.-F. Li, and D. Viehland, Phys. Rev. B **79**, 224301 (2009).